NUMERICAL SIMULATION OF FLOW AND FORCED CONVECTION HEAT TRANSFER IN CROSSFLOW OF INCOMPRESSIBLE FLUID OVER TWO ROTATING CIRCULAR CYLINDERS

Nikolay Pavlovich Moshkin*and Jakgrit Sompong

Received: Aug 20, 2009; Revised: Oct 13, 2009; Accepted: Oct 20, 2009

Abstract

In this paper, the problem of laminar two dimensional heat transfer from two rotating circular cylinders in cross flow of incompressible fluid under isothermal boundary condition is investigated. The study is based on the numerical solution of the full conservation equations of mass, momentum and energy for Reynolds numbers (based on cylinder diameter and velocity of uniform stream) up to 40 while Prandtl number ranges between 0.7 and 50. For the range of parameters considered, the study revealed that the rate of heat transfer decreases with the increase of speed of cylinders rotation for the gap between cylinders more than one diameter. The increase of Prandtl number resulted in an appreciable increase in the average Nusselt number. The streamlines and isotherms are plotted for a number of cases to show the details of the velocity and thermal fields.

Keywords: Heat transfer, flow over two rotating cylinders, incompressible fluid, finite difference method

Introduction

The flows of fluid and forced convection across a heated bluff body have been the subject of considerable research interest because of their relevance to many engineering applications. The flow past a cylinder is considered to be an ideal bluff body by which to study the important phenomena of heat and mass transfer. For instance, the knowledge of the hydrodynamic forces experienced by submerged cylindrical objects such as off-shore pipelines is essential for the design of such structures. Furthermore, because of changing process and climatic conditions, one also needs to determine the rate of heat transfer from such structures.

Heat transfer and fluid flow around a single rotating cylinder has been studied by several researchers, see for example recent works of Badr *et al.* (1989); Kang *et al.* (1999); Mahfouz and Bard (1999a, 1999b); Stojković *et al.* (2002); Mittal and Kumar (2003); Gshwendtner (2004).

The heat transfer and flow around two stationary or rotating circular cylinders can be

Institute of science, School of Mathematics, Suranaree University of Technology, Nakhon Ratchasima, Thailand
E-mail: moshkin@math.sut.ac.th
* *Corresponding author*

considered as an elementary flow which is helpful in understanding the flow patterns, heat transfer mechanism, and hydrodynamic characteristics around multiple bluff bodies in engineering practice.

Numerical computations for the flow over multiple cylinders have intensified during the last decade of the previous century. Chang and Song (1990) used a vorticity-stream function method to compute the flow past a pair of cylinders in side-by-side and tandem arrangements at $Re = 100$. Flow visualization and force coefficients were shown to be in good agreement with experiments. Mittal *et al.* (1997) used a finite element method to simulate three configurations, side-by-side, tandem and staggered arrangements of the cylinder pair at $Re = 100$ and 1000. Again, the results compared well with experiments. Recently, Kang (2003) investigated numerically the characteristics of flow around two side-by-side circular cylinders in the range of low Reynolds number defines as $Re = U_\infty D/\nu$ (where U_∞ and ν are the free-stream velocity and kinematic viscosity, respectively) over the range of $40 \leq Re \leq 160$, respectively, and the normalize gap spacing $g^* < 5$; he identified six kinds of wake patterns ($g^* = g / D$, where g and D are the distance between two cylinders surfaces and the cylinder diameter, respectively).

The problem of flow pass two rotating cylinders in side-by-side arrangement has not been investigated widely. Papers of Sungnul and Moshkin (2006, 2008) are devoted to study the self-motion of two rotating circular cylinders. Only two recent studies (Yoon *et al.*, 2007, 2009) have been found that investigate the flow around two rotating circular cylinders in side-by-side arrangement in the range of $|\alpha| \leq 2$ for various gap spacing at $Re = 100$ (α is the rotational speed at the cylinder surface normalized by the free-stream velocity). Only one paper of Joucaviel *et al.* (2008) has been found, which studies the thermal behavior of an assembly of rotating cylinders aligned in a cross-flow.

As described above, the effect of rotation for a single cylinder and of the gap spacing between two cylinders at rest in side-by-side arrangement on the corresponding flow and heat transfer has been studied by numerous researchers. Only a few researchers have studied the problem of flow pass two rotating cylinders in a side-by-side arrangement. However, the heat transfer and fluid flow past a pair of rotating circular cylinders in side-by-side arrangement have not been addressed at all. This paper presents a numerical investigation of the characteristics of the two-dimensional heat transfer and the laminar flow around two rotating circular cylinders in side-by-side arrangements. In order to consider the combined effects of rotation and spacing between the two cylinders on the flow and heat transfer, numerical simulations are performed at a various range of absolute rotational speeds ($|\alpha| \leq 2.5$), for different gap spacing and Reynolds number in the range $Re \leq 40$. Quantitative information about the flow and the heat transfer variables such as the local and average Nusselt number, pressure and friction coefficients on the cylinder surfaces is highlighted. The patterns of the flow and temperature fields are analyzed for a wide range of parameters.

The mathematical formulation of the heat/mass transfer problem of a flow past two rotating circular cylinders is described in the next section. The problem is recast in terms of a cylindrical bipolar coordinate system. The following sections present the details of the numerical algorithm based on the projection method to approximate the solution of the momentum equation, and the fractional step stabilizing correction method to approximate the solution of the energy equation. The validation of the numerical algorithm was done by comparing our computational results for large gap between the cylinders with available numerical and experimental data for flow and heat transfer over a single cylinder. The results of the various numerical experiments are reported and discussed in the final part of our paper.

Mathematical Formulation of the Problem

Consider the flow of a viscous incompressible fluid along the y-direction normal to the line

between the centers of two rotating circular cylinders with a constant velocity and temperature at infinity, U_∞, T_∞. The cylinders rotate about their axes at angular velocities ω_L and ω_R, assuming that a positive value corresponds to counter-clockwise rotation. A sketch of the flow geometry, coordinate system and notations are shown in Figure 1.

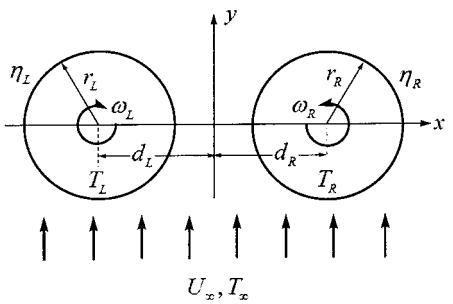

Figure 1. Schematic representation of the flow and heat transfer over a pair of rotating circular cylinders in side-by side arrangement

The present study is restricted to long cylinders and low Reynolds number, $Re \leq 40$. The flow across the cylinders is steady and two-dimensional. All flow variables are functions of the coordinates, x and y alone. The thermodynamical properties of the fluid (density, specific heat capacity c_p, thermal conductivity k) are assumed to be independent of temperature. Under these conditions, the momentum and energy equations are not coupled.

For the study of heat transfer and fluid flow around two cylinders, the cylindrical bipolar coordinate system is the most suited. The ubiquitous definition of the cylindrical bipolar coordinates (ξ, η, z) is

$$x = \frac{a \sinh \eta}{\cosh\eta - \cos\xi},$$

$$y = \frac{a \sin \xi}{\cosh\eta - \cos\xi}, \quad z = z, \tag{1}$$

where $\xi \in [0, 2\pi), \eta \in (-\infty, \infty)$ and $z \in (-\infty, \infty)$, $a > 0$ is the characteristic length in the cylindrical bipolar coordinates (so-called "focal distance"). The following identities show that curves of constant ξ and η are circles in the xy -space

$$x^2 + (y - a\cot\xi)^2 = a^2 \csc^2 \xi,$$

$$(x - a\coth\eta)^2 + y^2 = a^2 \mathrm{csch}^2 \eta. \tag{2}$$

Figure 1 shows the two cylinders described by $\eta = \eta_R$ (with $\eta_R > 0$) and $\eta = \eta_L$ (with $\eta_L < 0$), respectively. The cylinders' radii r_L and r_R and the distances of their centers from the origin d_L and d_R are given by

$$r_i = a\,\mathrm{csch}\,|\eta_i|,$$

$$d_i = a\coth|\eta_i|, \quad i = L, R \tag{3}$$

The center-to-center distance between the cylinders is equal to $d = d_L + d_R$. If $r_L + r_R$ and d are given, one can find a, η_L and η_R from relations (1)-(3) as follows

$$\eta_{R,L} = \ln\left[\frac{d^2 + r_R^2 - r_L^2}{2dr_R} \pm \sqrt{\left(\frac{d^2 + r_R^2 - r_L^2}{2dr_R}\right)^2 - 1}\,\right],$$

$$a = \sqrt{\frac{d^4 - 2d^2(r_R^2 + r_L^2) + (r_R^2 - r_L^2)^2}{4d^2}} \tag{4}$$

The fluid flow is governed by the conservation laws of momentum, mass and energy. The nondimensional form of the governing equations in the cylindrical bipolar coordinate system are

$$\frac{\partial v_\xi}{\partial t} + \frac{1}{h}\left(v_\xi \frac{\partial v_\xi}{\partial \xi} + v_\eta \frac{\partial v_\xi}{\partial \eta}\right) - \frac{1}{a}\left(v_\xi v_\eta \sinh\eta - v_\eta^2 \sin\xi\right) = -\frac{1}{h}\frac{\partial p}{\partial \xi}$$

$$+ \frac{1}{h}\frac{2}{Re}\left[\frac{1}{h}\left(\frac{\partial^2 v_\xi}{\partial \xi^2} + \frac{\partial^2 v_\xi}{\partial \eta^2}\right) - \frac{2}{a}\left(\sinh\eta \frac{\partial v_\eta}{\partial \xi} - \sin\xi \frac{\partial v_\eta}{\partial \eta}\right)\right.$$

$$\left. - \frac{\cosh\eta + \cos\xi}{a} v_\xi\right], \tag{5}$$

$$\frac{\partial v_\eta}{\partial t} + \frac{1}{h}\left(v_\xi \frac{\partial v_\eta}{\partial \xi} + v_\eta \frac{\partial v_\eta}{\partial \eta}\right) + \frac{1}{a}\left(v_\xi^2 \sinh\eta - v_\xi v_\eta \sin\xi\right) = -\frac{1}{h}\frac{\partial p}{\partial \eta}$$

$$+ \frac{1}{h}\frac{2}{Re}\left[\frac{1}{h}\left(\frac{\partial^2 v_\eta}{\partial \xi^2} + \frac{\partial^2 v_\eta}{\partial \eta^2}\right) + \frac{2}{a}\left(\sinh\eta \frac{\partial v_\xi}{\partial \xi} - \sin\xi \frac{\partial v_\xi}{\partial \eta}\right)\right.$$

$$\left. - \frac{\cosh\eta + \cos\xi}{a} v_\eta\right], \tag{6}$$

$$\frac{1}{h^2}\left(\frac{\partial(hv_\xi)}{\partial\xi}+\frac{\partial(hv_\eta)}{\partial\eta}\right)=0, \tag{7}$$

$$\frac{\partial T}{\partial t}+\frac{1}{h}\left(v_\xi\frac{\partial T}{\partial\xi}+v_\eta\frac{\partial T}{\partial\eta}\right)=\frac{2}{RePr}\frac{1}{h^2}\left(\frac{\partial^2 T}{\partial\xi^2}+\frac{\partial^2 T}{\partial\eta^2}\right), \tag{8}$$

where v_ξ and v_η are the velocity components in ξ and η directions, respectively, p is the pressure, t is the time, T is the fluid temperature, and $h = a/(\cosh\eta - \cos\xi)$. In the above equations all quantities are rendered dimensionless, the velocities by means of the free stream velocity U_∞, all lengths by means of the radius r_R of right cylinder, time by r_R/U_∞, pressure by ρU_∞^2 and temperature by $(T - T_\infty)$ $(T_R - T_\infty)$. The two nondimensional parameters which appear in the above equations are *Reynolds number*, $Re=\frac{2\rho U_\infty r_R}{\mu}$, and *Prandtl number*, $Pr=\frac{c_p\mu}{k}$ where μ is the viscosity of the fluid, ρ is the fluid density. On the cylinder surfaces the constant temperature condition and the no-slip condition for the velocity vector are imposed. The constant streamwise velocity and the uniform temperature are specified at infinity.

Discretization of the Governing Equations

Description of Grid

The computational domain is divided into a mesh by points $\xi_j = (j - 0.5)\Delta\xi$ and $\eta_i = \eta_L + (i - 0.5)\Delta\eta$ where $\Delta\xi = 2\pi/N$, $\Delta\eta = (\eta_R - \eta_L)/M$ are spatial mesh sizes in both ξ and η directions, respectively. A staggered placement of variables is used with velocity components $u = v_\eta$ located on the vertical sides of each cell and components $v = v_\xi$ on the horizontal sides of each cell. We used the fractional indexes to denote grid values of velocity components $u_{i+1/2,j} = u(\eta_{i+1/2j}, \xi_j)$ and $v_{i,j+1/2} = v(\eta_i, \xi_{j+1/2})$ where $\eta_{i+1/2,} = \eta_i + 0.5\Delta\eta$, $\xi_{j+1/2} = \xi_j + 0.5\Delta\xi$. The pressure p and temperature T are represented at cell centers, $p_{i,j} = p(\eta_i, \xi_j)$, $T_{i,j} = T(\eta_i, \xi_j)$. The upper index n denotes values of variables at time $t_n = n\tau$ where τ is the step size in time.

Discretization of Navier-Stokes Equations

Simulating incompressible flows presents a difficulty of satisfying the property of mass conservation. The velocity field must satisfy the incompressibility constraint, which reflects the unability of pressure to do compression work. For developing numerical approximations to this problem, it is natural to exploit the techniques of the fractional step projection method of Chorin (1968). The main idea of the fractional step projection method is the splitting of the viscosity effect from the incompressibility, which are dealt with in two separate subsequent steps.

The time derivatives are represented by forward differences. In case of a steady solution, time is considered as artificial (iterative) time. If the integer n represents the time level, then the intermediate velocity field can be calculated from

$$\tilde{v}_{i,j+\frac{1}{2}} = v^n_{i,j+\frac{1}{2}} - \tau(CONV)^n_{i,j+\frac{1}{2}} + \tau\frac{2}{Re}(DIFFV)^n_{i,j+\frac{1}{2}}, \tag{9}$$

$$\tilde{u}_{i+\frac{1}{2},j} = u^n_{i+\frac{1}{2},j} - \tau(CONU)^n_{i+\frac{1}{2},j} + \tau\frac{2}{Re}(DIFFU)^n_{i+\frac{1}{2},j}. \tag{10}$$

Here we used the following notation for convective and diffusive terms

$$CONV = \frac{1}{h}\left(v\frac{\partial v}{\partial\xi}+u\frac{\partial v}{\partial\eta}\right)-\frac{1}{a}\left(vu\sinh\eta - u^2\sin\xi\right),$$

$$CONU = \frac{1}{h}\left(v\frac{\partial u}{\partial\xi}+u\frac{\partial u}{\partial\eta}\right)+\frac{1}{a}\left(v^2\sinh\eta - vu\sin\xi\right),$$

$$DIFFV = \frac{1}{h}\left\{\frac{1}{h}\left[\frac{\partial^2 v}{\partial\xi^2}+\frac{\partial^2 v}{\partial\eta^2}\right]-\frac{2}{a}\left(\sinh\eta\frac{\partial u}{\partial\xi}-\sin\xi\frac{\partial u}{\partial\eta}\right)+\frac{\cosh\eta+\cos\xi}{a}v\right\},$$

$$DIFFU = \frac{1}{h}\left\{\frac{1}{h}\left[\frac{\partial^2 u}{\partial\xi^2}+\frac{\partial^2 u}{\partial\eta^2}\right]+\frac{2}{a}\left(\sinh\eta\frac{\partial v}{\partial\xi}-\sin\xi\frac{\partial v}{\partial\eta}\right)-\frac{\cosh\eta+\cos\xi}{a}u\right\}$$

The second order central difference scheme has been used to discretize both the convective and diffusive terms. The velocity components $\tilde{v}_{i,j+\frac{1}{2}}$ and $\tilde{u}_{i+\frac{1}{2},j}$ are computed for

all faces of the cells except one, where the velocity components are given by the boundary condition. Figure 2 shows the location of grid points where velocity components are known from the no-slip boundary condition or from the boundary condition at infinity. The boundary condition at infinity is shifted on the boundary of finite domains Ω_1 and Ω_2.

The explicit advanced tilde velocity may not necessarily lead to a flow field with zero mass divergence in each cell. This is because at this stage the pressure field not used. Pressure p^{n+1} and velocity components u^{n+1} and v^{n+1} have to be computed simultaneously in such a way that no net mass flow takes place in or out of a cell. In such case, we make use of an iterative correction procedure in order to obtain a divergence free velocity field. First, the velocity components are updated in the following form

$$v_{i,j+1/2}^{n+1,s} = \tilde{v}_{i,j+1/2} - \frac{\tau}{h_{i,j+1/2}} \left(\frac{p_{i,j+1} - p_{i,j}}{\Delta\xi} \right)^{n+1,s-1}, \qquad (11)$$

$$u_{i+1/2,j}^{n+1,s} = \tilde{u}_{i+1/2,j} - \frac{\tau}{h_{i+1/2,j}} \left(\frac{p_{i+1,j} - p_{i,j}}{\Delta\eta} \right)^{n+1,s-1}, \qquad (12)$$

where the index s is used to denote iteration number, $s = 1, 2, 3, \ldots$. In the case $s = 1$, we assume that $p^{n+1,0} = p^n$. The point iterative pressure equation becomes

$$p_{i,j}^{n+1,s} = p_{i,j}^{n+1,s-1} - \frac{\beta}{\tau} div(u,v)_{i,j}^{n+1,s}, \qquad (13)$$

where $div(u,v)_{i,j}^{n+1,s}$ is the unsatisfied divergence at the $(i, j)^{th}$ cell due to incorrect velocities $\tilde{u}_{i+1/2,j}^{n+1}$ and $\tilde{v}_{i,j+1/2}^{n+1}$.

The pressure (velocity) equations (11)-(13) are to be iterated until the continuity equation is satisfied to the prescribed accuracy and then the computation proceed to next time step (artificial time)

$$div(u,v)_{i,j}^{n+1,S} \le 10^{-6}, \qquad (14)$$

where the discretized form of continuity equation is

$$div(u,v)_{i,j}^{n+1,s} = \frac{1}{h_{i,j}^2} \left[\frac{(hv)_{i,j+1/2}^{n+1,s} - (hv)_{i,j-1/2}^{n+1,s}}{\Delta\xi} + \frac{(hu)_{i+1/2,j}^{n+1,s} - (hu)_{i-1/2,j}^{n+1,s}}{\Delta\eta} \right]. \qquad (15)$$

The optimal value of the relaxation parameter β was found by trial and error.

The pressure advanced equation (13) can be interpreted as Jacobi iterative method to

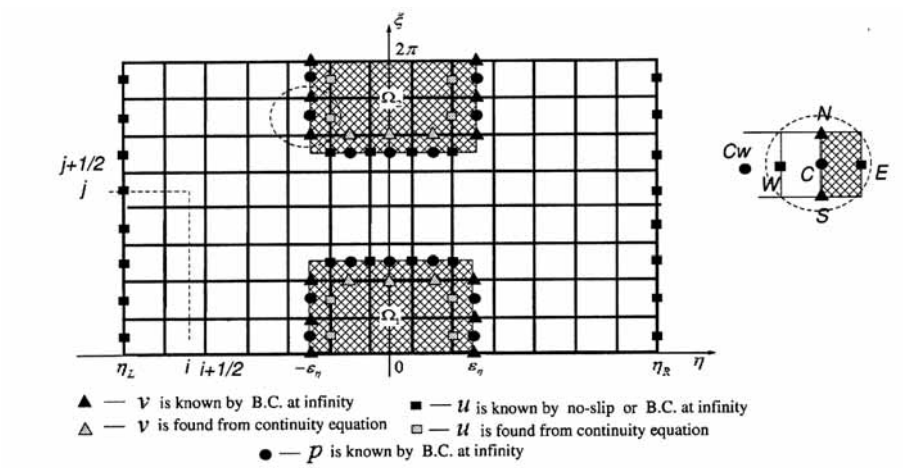

Figure 2. Sketch of computational grid and implementation of boundary condition

solve the finite-difference analog of Poisson equation for pressure. Let iterative process converges, i.e. $v^{n+1}= v^{n+1,s}$, $u^{n+1}= u^{n+1,s}$, and $p^{n+1}= p^{n+1,s}$. Substituting (11) and (12) into (15) and requiring that $div(u,v)_{i,j}^{n+1} \equiv 0$, we get the following finite-difference approximation of Poisson equation for pressure,

$$div(\nabla p^{n+1})_{i,j} = \frac{1}{\tau} div(\tilde{u},\tilde{v})_{i,j}. \qquad (16)$$

Finite difference equation (16) is an algebraic system with respect to the unknown vector $[..., p_{i-1,j}^{n+1}, p_{i,j}^{n+1}, p_{i+1,j}^{n+1}, p_{i,j-1}^{n+1}, p_{i,j+1}^{n+1}, ...]$. System of equations (16) can be solved by the method of false transient

$$\left(\frac{\partial p^{n+1}}{\partial \beta}\right) = div(\nabla p^{n+1}) - \frac{1}{\tau} div(\tilde{u},\tilde{v}), \qquad (17)$$

where β is an iterative parameter. Equation (13) is a particular case of (17) where the forward finite difference is used to approximate the left-hand-side in (17),

$$\left(\frac{\partial p^{n+1,s+1}}{\partial \beta}\right)_{i,j} \approx \frac{p_{i,j}^{n+1,s+1} - p_{i,j}^{n+1,s}}{\beta}. \qquad (18)$$

On the surface of the cylinders, the no-slip condition is applied, which is equivalent to setting the tangential velocity at the boundary to α_i, $i = L, R$ and the normal velocity to zero. Where α_i is defined as $\alpha_i = \omega_i D / 2U_\infty$, ($\omega_i$ is the angular velocity of the cylinders). Implementation of no-slip and no-penetration boundary conditions is straightforward. Because of the staggered arrangement of the variables, we used the second order one-side finite differences to approximate the derivatives $\frac{\partial v}{\partial \eta}$ and $\frac{\partial^2 v}{\partial \eta^2}$.

In a numerical simulation, it is impossible to satisfy constant streamwise velocity as $x^2 + y^2 \to \infty$. Usual practice involves the placement of the conditions at a faraway ("artificial") boundary, which is located at a large distance from the body. In our computations, the far boundary coincides with lines $\xi = const$ and $\eta = const$ (recall that images of the infinity in computational domain are two points ($\xi = 0$, $\eta = 0$) and ($\xi = 2\pi$, $\eta = 0$) . To be more exact, we choose far boundary as the boundary of the following domain

$$\Omega_1 = \{(\xi,\eta) \mid (\eta = \pm\varepsilon_\eta \text{ and } 0 \le \xi \le \varepsilon_\xi) \cup (\xi = \varepsilon_\xi \text{ and } -\varepsilon_\eta \le \eta \le \varepsilon_\eta)\},$$

$$\Omega_2 = \{(\xi,\eta) \mid (\eta = \pm\varepsilon_\eta \text{ and } 2\pi - \varepsilon_\xi \le \xi \le 2\pi) \cup (\xi = 2\pi - \varepsilon_\xi \text{ and } -\varepsilon_\eta \le \eta \le \varepsilon_\eta)\},$$

where $\varepsilon_\eta = \pm(k_w + 0.5)\Delta\eta$, $\varepsilon_\xi = \pm(k_d + 0.5)\Delta\xi$, and k_w, k_d are integer numbers. In Figure 2 a sketch of these domains Ω_1 and Ω_2 is shown by shadow regions.

At the nodes of the mesh which are located on the boundary of the regions Ω_1 and Ω_2 we assumed that the tangent component of velocity vector and pressure $p = p_\infty$ are known.

$$v = -(u_x)_\infty \frac{h}{a}\sinh\eta\sin\xi + (u_y)_\infty \frac{h}{a}(\cosh\eta\cos\xi - 1),$$

$$\left(/\text{or} \quad u = -(u_y)_\infty \frac{h}{a}(\cosh\eta\cos\xi - 1) - (u_y)_\infty \frac{h}{a}\sinh\eta\sin\xi\right).$$

Here we have utilized the idea that prescribing tangent component of velocity and pressure gives a well-posed problem for the Navier-Stokes equations (Antontsev *et al.* (1990), Moshkin and Yambangwai (2009)). The normal to the boundary component of the velocity vector is computed from the requirement of continuity equation for the cells contained in this boundary. For example, for the case shown in Figure 2 the boundary of region Ω_1 (/or Ω_2) passes through points 'N', 'S', and 'C'. The tangential component of velocity v_N^{n+1} and v_S^{n+1} are given by boundary condition as well as the pressure at point 'C' is equal to pressure at infinity. The component of velocity vector u_E^{n+1} is computed from the requirement of zero divergence for the cell centered at the point 'C'

$$\frac{u_E^{n+1}-u_W^{n+1}}{\Delta\eta}+\frac{v_N^{n+1}-v_S^{n+1}}{\Delta\xi}=0,$$

$$u_E^{n+1}=\tilde{u}_W-\frac{\tau}{h_w}\left(\frac{p_C-p_{Cw}}{\Delta\eta}\right)^{n+1}-\frac{\Delta\eta}{\Delta\xi}(v_N^{n+1}-v_S^{n+1}).$$

Discretization of the Energy Equation

The momentum and energy equations are not coupled. The energy equation is solved separately from the Navier-Stokes equations. When the steady solution of Navier-Stokes equations is computed, the iterative method of stabilizing correction is used (Yanenko, 1971) to find the steady distribution of temperature. The structure of the scheme of stabilizing correction is the following:

• the first fractional step produces absolute consistency with the energy equation,

• all succeeding fractional steps are corrections and serve to improve the stability.

For the 2D case, the scheme possesses strong stability and satisfies the property of complete consistency. The requirement of complete consistency guarantees convergence of the unsteady solution to the steady solution for arbitrary time and space step size (Yaneko 1971).

To describe the scheme of stabilizing correction, consider a two dimensional convection-diffusion equation in the form

$$(\vec{v}\cdot\nabla)T=\frac{2}{RePr}\Delta T, \qquad (19)$$

where $T=T(\xi,\eta),\vec{v}=(v_\xi,v_\eta),\nabla$ is the gradient operator, and ∇ is the Laplace operator. To find the steady solution of (19) we use the method of false transient. Consider the related unsteady problem with "fiction" time

$$\frac{\partial T}{\partial t}=\Lambda_1 T+\Lambda_2 T, \qquad (20)$$

where Λ_1,Λ_2 represent the derivatives in only one space direction. For the solution of (20) Douglas and Rachford (1956) proposed the following scheme

$$\frac{T^{k+1/2}-T^k}{\tau}=\Lambda_1 T^{k+1/2}+\Lambda_2 T^k, \qquad (21)$$

$$\frac{T^{k+1}-T^{k+1/2}}{\tau}=\Lambda_2(T^{k+1}-T^k). \qquad (22)$$

Eliminating $T^{k+1/2}$ we can rewrite system (21) and (22) in the following uniform scheme

$$\frac{T^{k+1}-T^k}{\tau}=\Lambda_1 T^{k+1}+\Lambda_2 T^{k+1}-\tau\Lambda_1\Lambda_2(T^{k+1}-T^k). \qquad (23)$$

It follows from this that scheme (21) and (22), and the equivalent scheme (23) approximate equation (20) with the same order of accuracy as the implicit scheme

$$\frac{T^{k+1}-T^k}{\tau}=\Lambda_1 T^{k+1}+\Lambda_2 T^{k+1}. \qquad (24)$$

Temperature references to nodes of main computational grid related with center of cells of discrete domain $\Omega_h=\{(\xi_j,\eta_i)\,|\,\xi_j=(j-0.5)\Delta\xi,\ \eta_i=\eta_L+(i-0.5)\Delta\eta,\ \ j=0,1,...,n+1,i=0,1,...,m+1\}$. On the boundary of the shadowed domains Ω_1 and Ω_2 the constant temperature of uniform stream $T = T_\infty$ is prescribed. The constant temperature at the cylinder surfaces is approximated by the following

$$\frac{T_{0,j}+T_{1,j}}{2}=T_L,\quad \frac{T_{m+1,j}+T_{m,j}}{2}=T_R,$$

where $T_{0,j}$ and $T_{m+1,j}$ are "ghost" points, which introduced for convenience in writing the computational code. For each fractional step a system of linear algebraic equation with tridiagonal matrix is solved.

Computation of Heat Transfer and Flow Characteristics

Two groups of characteristic quantities are of interest in the present study, one for characterizing the forces at the cylinder surface

and the other for the heat transfer. If F_{x_i} and F_{y_i}, $i = L, R$ are the lift and drag forces on the cylinders; the lift and drag force coefficients are defined by

$$C_{L_i} = \frac{F_{x_i}}{\rho U_\infty D}, C_D = \frac{F_{y_i}}{\rho U_\infty D}, \qquad i = L, R, \tag{25}$$

and each consists of components due to the friction forces and the pressure. Hence

$$C_L = C_{L_f} + C_{Lp}, \; C_D = C_{D_f} + C_{Dp}, \tag{26}$$

where

$$C_{L_p} = -\frac{1}{\rho U_\infty D}\int_\Sigma p\vec{n}\cdot\vec{i}_x \, dS,$$

$$C_{L_f} = -\frac{1}{\rho U_\infty D}\int_\Sigma \mu(\vec{n}\times\vec{\omega})\cdot\vec{i}_x \, dS,$$

$$C_{D_p} = -\frac{1}{\rho U_\infty D}\int_\Sigma p\vec{n}\cdot\vec{i}_y \, dS,$$

$$C_{D_f} = -\frac{1}{\rho U_\infty D}\int_\Sigma \mu(\vec{n}\times\vec{\omega})\cdot\vec{i}_y \, dS.$$

Here $\vec{i}_x, \vec{i}_y$ are the unit vectors in x and y axes directions, Σ is the cylinder perimeter, and $\vec{n}$ is the outward unit normal to surface vector. To evaluate the integrals we used the middle point rule, for example, in order to compute C_{D_p} we used formula:

$$C_{D_p}\Big|_i = \sum_{j=1}^{n}\left\{hp\left[\left(\frac{h}{a}(\cosh\eta\cos\xi - 1)\right)n_\xi + \left(\frac{h}{a} - \sinh\eta\sin\xi\right)n_\eta\right]\right\}_{i,j}\Delta\xi, \tag{27}$$

where $i = L, R$, that is, we computed the coefficient on the left and right cylinder surfaces, respectively. Pressure on the cylinder surfaces is evaluated by extrapolation from interior points.

The vorticity in the cylindrical bipolar coordinate system is given by the following formula

$$\omega = -\frac{1}{h}\left[\frac{\partial v}{\partial\eta} - \frac{\partial u}{\partial\xi} - \frac{h}{a}(v\sinh\eta - u\sin\xi)\right].$$

On the cylinder surfaces the tangent derivative is equal zero $\frac{\partial u}{\partial\xi} = 0$. The normal derivative $\frac{\partial v}{\partial\eta}$ is approximated by one-side second order finite-differences.

The important parameter of interest in heat transfer problems is the heat transfer rate per unit area from the cylinder wall to the ambient fluid. The local Nusselt number in the cylindrical bipolar coordinate system based on the diameter of the cylinder is

$$Nu = -\left(\frac{\partial T}{\partial n}\right) = -\nabla T\cdot\vec{n} = -\frac{1}{h}\frac{\partial T}{\partial\eta} = -\left(\frac{\cosh\eta - \cos\xi}{a}\right)\frac{\partial T}{\partial\eta}. \tag{28}$$

The average Nusselt number is calculated by averaging the local Nusselt number over the surface of the cylinder

$$\overline{Nu} = -\frac{1}{2\pi}\int_0^{2\pi}\frac{\partial T}{\partial\eta}d\xi, \qquad \xi\in[0, 2\pi]. \tag{29}$$

The integral is approximated by the middle point rule.

Validations

The first task in any numerical work is to validate the codes ability to accurately reproduce published experimental and numerical results. Unfortunately, there are no data in the literature to verify the accuracy of the considered problem (flow over two rotating cylinders). Since for large gap spacing between the cylinders, the mutual influence of the cylinders on each other is negligible we can assume that the flow and heat transfer will be similar to flow and heat transfer over a single cylinder. The comparisons with flow and heat

transfer around a single cylinder can be viewed as a partial validation of the algorithm presented. Thus, the comparisons were carried out of the characteristics of flow and heat transfer as obtained from our numerical results (gap spacing $g = 14$, $g = (d - r_L - r_R)/D_R$) with the published data for a single cylinder. All computations were performed in a large domain in order to reduce the influence of the outer boundary. A sequence of uniform grids is used. The wake behind a single cylinder is steady in the flow regime $Re \leq 46 \pm 1$. We assume that in the case of two rotating circular cylinders, the steady regime exists at least for the same range of the Reynolds numbers. Due to symmetry with respect to the y -axis, all our results are presented for the left cylinder only.

The important characteristics of flow are the drag coefficients, $C_D = C_{Df} + C_{Dp}$, the local and average Nusselt numbers. They are presented in Table 1 for Re = 20, g = 14, and Pr = 0.7. Table 1 shows convergence of our results on a sequence of grids and good agreement with results from other publications.

Representative results showing the variation of the pressure coefficient C_{Dp} and vorticity ω on the surface of the left cylinder are plotted in Figure 3 for the two values of the Reynolds number Re = 20 and 40 and for the gap spacing g = 14.

Comparison of our numerical simulations is performed with the numerical results of Dennis and Chang (1970) for Re = 20 and 40, with the experimental results of Thom for Re = 36, 45 and Apelt for Re = 40 (Batchelor, 2000). Our data come from simulations on the grid with 81 x 81 nodes in the ξ - η plane. The closest distance from the cylinder surfaces to the far boundary for this grid is 53 cylinder diameters. The angle variable θ is zero at the front stagnation point and increases in the clockwise direction on the left cylinder. The data

Table 1. Validations of the numerical algorithm. Effect of grid refinement upon C_D, C_{Dp}, C_{Di} and average Nusselt number $\overline{Nu}$ for Re = 20 and g = 14

Source	C_D,	C_{Dp},	C_{Di}	$\overline{Nu}$ (Pr = 0.7)
Present (21 x 21)	2.149	1.274	0.875	2.669
Present (41 x 41)	2.112	1.274	0.838	2.481
Present (81 x 81)	2.064	1.242	0.822	2.478
Soares (2005) *et al.*	2.035	1.193	0.842	2.430
Stålberg *et al.* (2006)	2.052	1.229	0.823	-
Bharti *et al.* (2007)	-	-	-	2.465

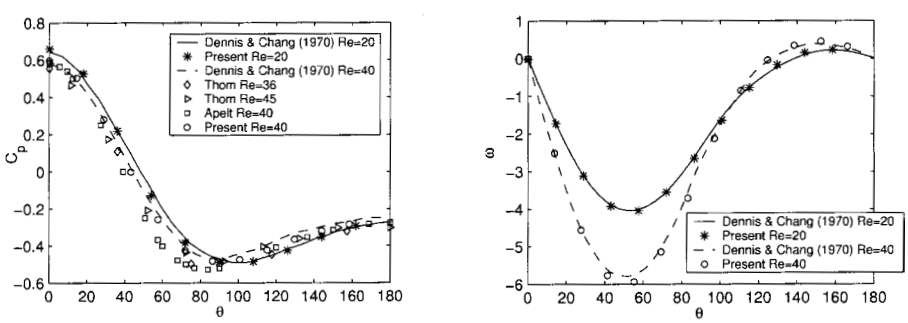

Figure 3. Validation of numerical algorithm (a)-pressure coefficient over cylinder surface, (b)-the vorticity distribution over cylinder surface, for the left cylinder at Re = 20, 40, and g = 14

from our simulations ($*$ - sign for $Re = 20$ and o - sign for $Re = 40$) match the results from other publications.

To the authors' knowledge, even for the flow past a single circular cylinder, there are only a few published sets of data pertaining to the drag and lift coefficients at $Re \leq 40$ and nonzero rotation. Table 2 shows comparisons of our numerical results for $Re = 20$, $g = 14$ with those numerically obtained by Badr *et al.* (1989); Ingham and Tang (1990); Sungnul and Moshkin (2006) and Chung (2006). The left cylinder rotates with constant angular velocity in clockwise direction and the right cylinder rotates with the same speed in counterclockwise direction. The validation results inspire confidence in the reliability and accuracy of the numerical method used.

Results

Numerical computations were carried out for $Re = 5 - 40$, for a range of values of Prandtl number from 0.7 to 20, for range of rotation $\alpha = 0.1 + 2.5$, and different gap spacing. In all cases we represent results obtained on a grid with 81 x 81 nodes in the computational domain. The influence of the gap spacing on the heat transfer rate in terms of the local Nusselt number $Nu(\theta)$ is shown by Figures 4(a) and 4(b) for $Re = 20$, $\alpha = 0$ and $Pr = 0.7$ and 20. These figures show that a significant influence of the distance between cylinders on the local Nusselt number $Nu(\theta)$ is observed for $g \lesssim 5$.

Table 2. Hydrodynamic parameters of flow over a rotating circular cylinder at $Re = 20$ with $g = 14$

Contribution	C_D			C_L		
	$\alpha = 0.1$	$\alpha = 1.0$	$\alpha = 2.0$	$\alpha = 0.1$	$\alpha = 1.0$	$\alpha = 2.0$
Present (21 x 21)	2.146	2.035	1.906	0.286	2.974	6.309
Present (41 x 41)	2.108	1.897	1.410	0.288	2.864	6.030
Present (81 x 81)	2.052	1.847	1.346	0.293	2.770	5.825
Sungnul & Moshkin (2006)	2.120	1.887	1.363	0.291	2.797	5.866
Badr et al. (1989)	1.990	2.000	—	0.276	2.740	—
Ingham et al.(1990)	1.995	1.925	1.627	0.254	2.617	5.719
Chung (2006)	2.043	1.888	1.361	0.258	2.629	5.507

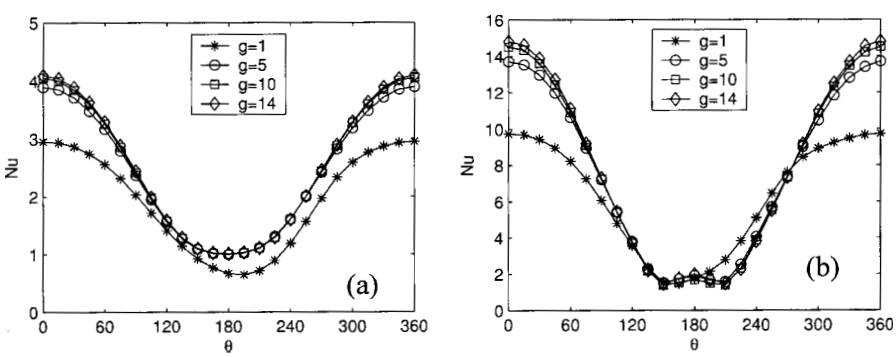

Figure 4. Local Nusselt number for different gap spacing at $Re = 20$, $\alpha = 0$, and (a)- $Pr = 0.7$, (b)- $Pr = 20$

Another aspect that seems to be interesting is the decreasing *Nu(θ)* for $0^\circ \lesssim \theta \lesssim 360^\circ$ with decreasing g in the case of $Pr = 0.7$ (rate of convection and conduction almost equal). In the case of $Pr = 20$ (convection is the dominant mechanism of heat transfer) *Nu(θ)* decreases with g decreasing for $0^\circ \lesssim \theta \lesssim 180^\circ$ and $270^\circ \lesssim \theta \leqslant 360^\circ$, and for $180^\circ \lesssim \theta \leqslant 270^\circ$ the values of *Nu(θ)* increases with g decreasing. It is not surprised that the average Nusselt number for each individual cylinder increases with increasing gap spacing and tends to the average Nusselt number for a single cylinder. Figure 5 shows the variation of the average Nusselt number with gap spacing between non-rotating cylinders at different Prandtl numbers and fixed Reynolds number, $Re = 20$.

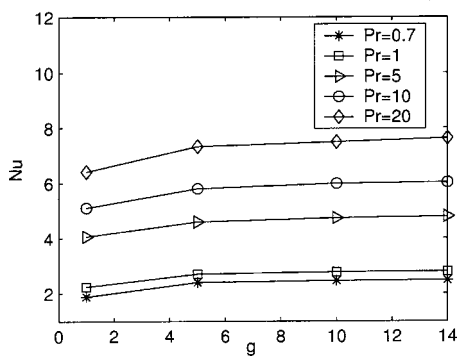

Figure 5. Average Nusselt number for different gap spacing at $Re = 20$, $\alpha = 0$

As expected, the average Nusselt number for the cylinders increases with the Prandtl number.

Large Gap Spacing

The effect of steady rotation of the cylinders on heat transfer is first studied for large gap spacing, $g = 14$. Figure 6 shows the variation of the local Nusselt number *Nu(θ)* at $Re = 20$, $Pr = 0.7$ and $Pr = 20$, and for different values of α ($\alpha \in [0,2]$). An increase in the rotation of the cylinders leads to a displacement of the points of maximum and minimum Nusselt number in the direction of rotation. At the same time, the maximum value of the local Nusselt number decreases with increase of rotational speed. The minimum value of the local Nusselt number slightly increases in step with increasing rotation. For $Pr = 20$ and high rotational speed $\alpha = 2$, the rate of heat transfer around the cylinder surface becomes almost uniform as shown in Figure 6(b). This behavior is quite expected, since due to the no-slip condition the fluid layer adjacent to the cylinder enwraps the cylinder and rotates with almost the same angular velocity. Increasing rotational speed to $\alpha = 2$ creates a thick rotating layer (buffering layers) around the cylinder. The heat transfer through that layer is mostly due to thermal conduction.

Figure 7 shows streamline patterns and temperature contours plot for large gap spacing $g = 14$, Reynolds number $Re = 20$,

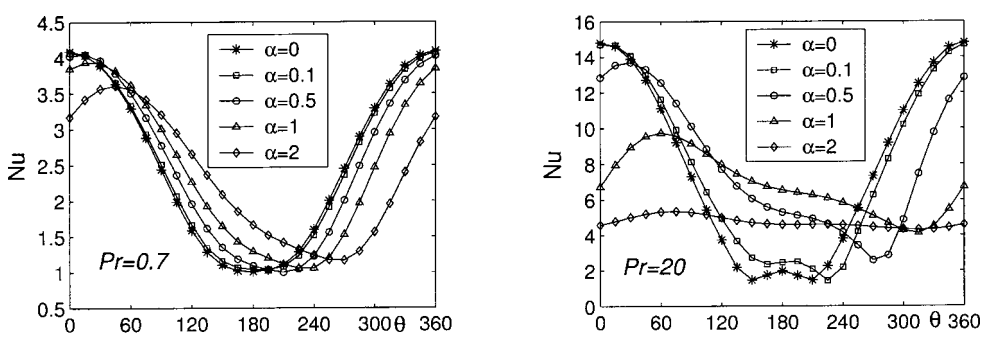

(a) (b)

Figure 6. Local Nusselt number variation on the surface of the circular cylinders at $Re = 20$, $Pr = 20$, $Pr = 0.7$ and 20, $g = 14$ for $\alpha = 0$, 0.1, 0.5, 1.0, and 2.0

Pr = 0.7, 20, and α = 0.1, 1.0, 2.0. The rotation effect substantially changes the flow pattern in the vicinity of the cylinder. Without rotation, the flow field exhibits a symmetric pair of standing vortices behind the cylinder defining a closed recirculation region. With the increase of the rotation rate, the flow becomes asymmetric: the vortex detaches from the cylinder and the stagnation point rotates in the direction opposite to the direction of cylinder rotation departing from the surface of the cylinders (see first row in Figure 7).The minimum of the local Nusselt number is observed near this point. In downstream direction, the streamlines are shifted clockwise and the same occurs for the isotherms (see second and third rows in Figure 7) resulting in the asymmetrical distribution of the local Nusselt number as shown in Figure 6. The oncoming fluid stream is accelerated by the rotating cylinder on the "west' side of an egg-shaped region of closed streamlines. As a result, the convective heat transfer between the ambient fluid and the fluid within the egg-shaped region is increased at the point of maximum velocity. This observation explains the deviation of the maximum of the local Nusselt number in the direction of cylinder's rotation. An increase in the Prandtl number increases the compactness of the isothermals toward the downstream direction (compare second and third rows of Figure 7). Owing to rotation a wake-shapes region of

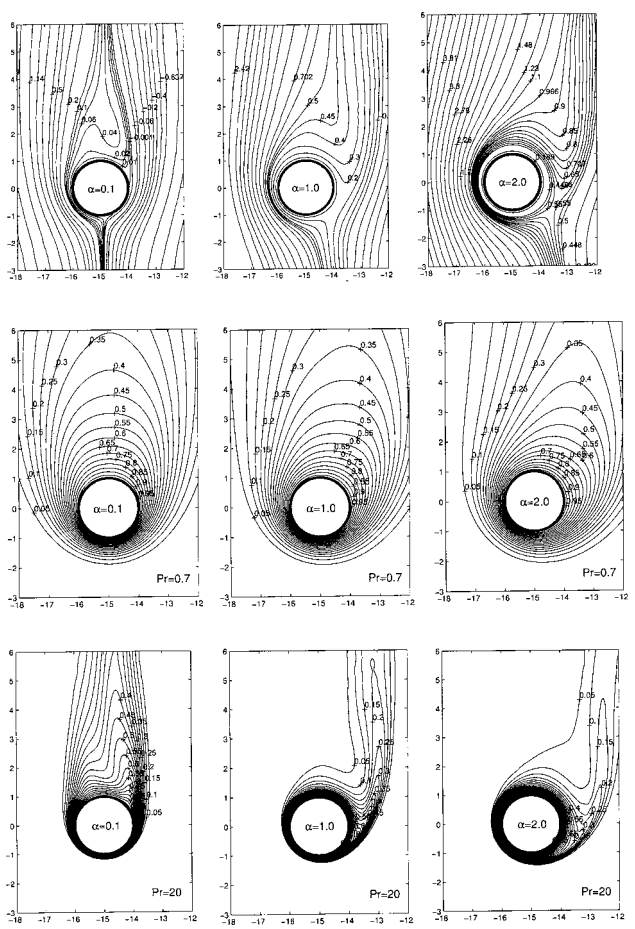

Figure 7. Streamline patterns (first row), temperature contours over two circular cylinders at *Re* = 20, *g* = 14, α = 0.1, 1.0 amd 2.0 and for *Pr* = 0.7, (second row) and *Pr* = 20 (third row)

is otherms is shifted in the clockwise direction for the left-hand side cylinder (see third row in Figure 7) and in the counterclockwise direction for the right-hand side cylinder. This behavior can be explained by the increasing role of convection in the mechanism of heat transfer with increasing *Pr* number. We remind here that we represent results only for left-hand side cylinder, which rotates in the clockwise direction.

Figure 8(a) shows the dependence of the average Nusselt number on the rotational speed for $Re = 20$, $g = 14$ and $Pr = 0.7, 1.0, 5.0, 10.0$, and 20.0. The average Nusselt number decreases with increasing α. In the case $Pr = 1$ the average Nusselt number drops down by 10% and in the case of $Pr = 20$ drops down by almost 50% when α increases from 0 up to 2. This behavior can be explained by the fluid layers adjacent to the rotating cylinders due to no-slip requirement.

Small Gap Spacing

For small gap spacing, $g = 1$, the effect of rotational speed is shown in Figures 8-12, for $Re = 10$ and 20, $Pr = 0.7$ and 20.0, and α in the range 0 - 2.5. Representative plots of the streamlines and isotherms for $Re = 10$ and 20, $g = 1$, $Pr = 0.7$, 10 and 20, and $0.5 \leq \alpha \leq 20$ are shown in Figures 9-11. Due to the no-slip requirement, there are regions of closed streamlines near the cylinders for all values of α. The size of these regions increases with increasing rotational speed. At some $\alpha = \alpha^*$ the two regions merge together. The main stream flows around the fluid region, which surrounds both cylinders and consists of two regions of closed streamlines. These regions acts as a buffer (blanket) isolating both cylinders from the main stream and causing a decrease in the overall heat transfer rate from the cylinder surfaces. The values of $\alpha*$ depends on Reynolds number. As can be seen from Figure 9 for $Re = 10$ and $\alpha = 0.5$ main stream can not pass through gap between cylinders, however for $Re = 20$ and $\alpha = 0.5$ main stream is strong enough to go through the gap between two cylinders. A further increase in angular velocity $\alpha > \alpha^*$ is a reason of further increasing of regions size in both *x* and *y* directions. The stagnation points are now located on the y – axis, both upstream and downstream, as illustrated in Figure 9.

The details of the steady thermal fields are presented in Figures 10 and 11 (for the cases of $Re = 10$ and 20, $g = 1$, $Pr = 1$, 10, 20, and $\alpha = 0.5, 1.0, 1.5$, and 2.0) in the form of constant temperature contours. Isotherm patterns depend on the Prandtl number. For $Re = 20$, $Pr = 20$ and $\alpha = 0.5$ there are two almost separate wake-type isotherm patterns downstream of each cylinders. One of the interesting features of the temperature field is topological similarity of isotherm patterns in cases of $\alpha = 1.5$ and $\alpha = 2.0$. For the cases of large Prandtl numbers $Pr = 40$ and 20, the convection is dominant mechanism in heat transfer. The lines of constant

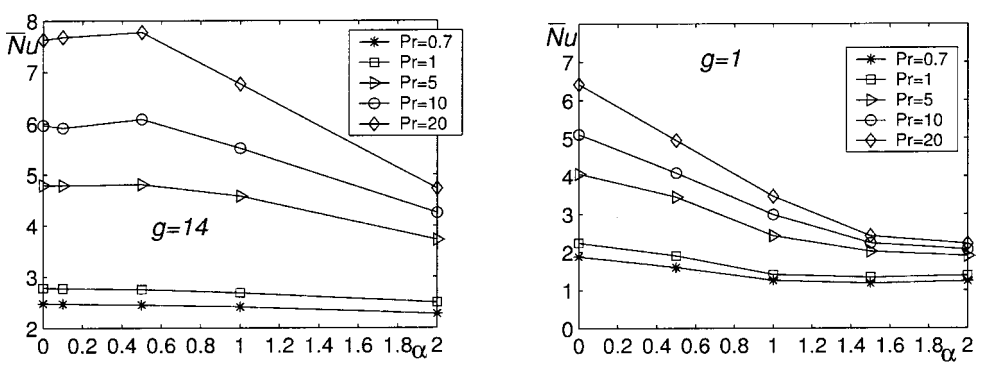

Figure 8. Average Nusselt number at $Re = 20$, (a)-$g = 14$ and (b)- $g = 1$, for different Prandtl numbers

temperature in the regions of closed streamlines follow to the streamlines contours. Heat exchange from the cylinders to the main stream occurred through the boundary of the fluid region, which enwraps both cylinders. Heat transfer inside this region is mostly due to conduction. By this reason, the average Nusselt number almost does not change for α >1.5 as can be seen from Figure 8(b). Comparison of isotherms in Figures 10 and 11 shows that an increase in Prandtl number makes wake-shape region of temperature field more narrow downstream behind the cylinder It is interesting to point out that the rate of rotation does not significantly affect the size of the wake-shaped region.

Another interesting observation is the location of the saddle critical point in the temperature field. This critical point is located on the line connecting the cylinder centers in the cases of Re =10, α = 0.5, Pr = 0.7, and

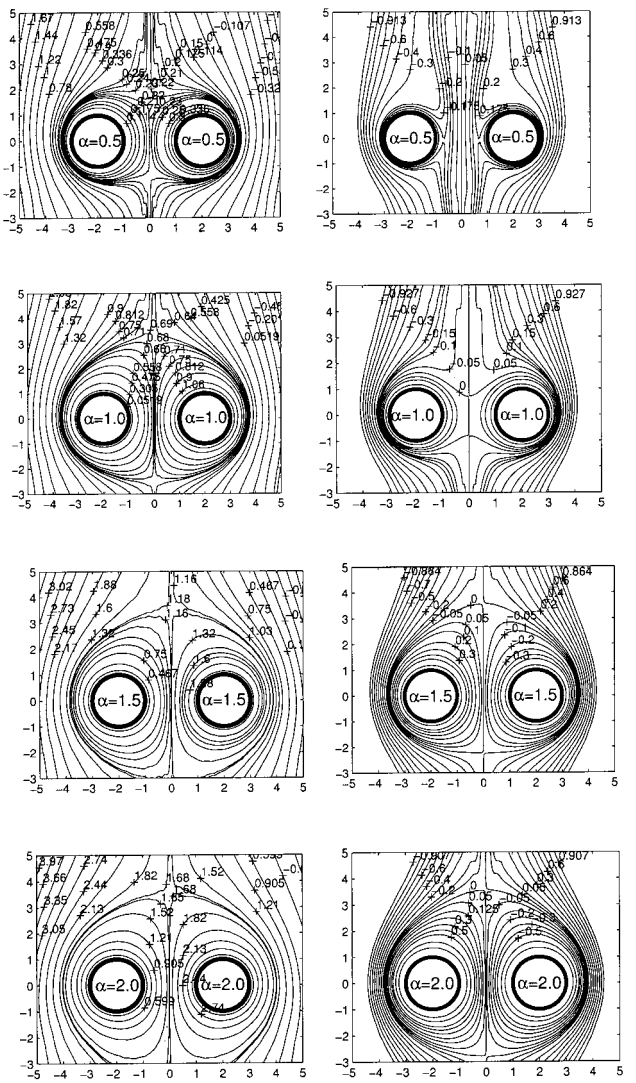

Figure 9. Streamlines contours over two circular cylinders at *Re* = 10 left column and *Re* = 20 right column *Pr* = 1, *g* = 1, and α = 0.5, 1.0, 1.5, and 2.0

Re = 20, α = 1.0, Pr = 0.7. For larger values of α, α >1.5 the saddle point is shifted down (in the negative direction of y-axis) by the fluid layers which rotate in step with cylinders due to no-slip condition.

Figure 12 shows effect of rotation on heat transfer in terms of the local Nusselt number distribution. For Pr = 20 and α = 2.5 the local Nusselt number is almost constant on the cylinder surfaces. As a result, the average Nusselt number drops as α increase. Dependence of the average $\overline{Nu}$ number on rotational speed is demonstrated in Figure 8(b). Figure 8(b) shows that for $0 < \alpha \lesssim 1.5$, $\overline{Nu}$ decreases sufficiently fast, whereas for $\alpha \gtrsim 1.5$ the rate of decrease of $\overline{Nu}$ is very low. This allows us to assume that heat transfer is almost insensitive to the speed of rotation if $\alpha \gtrsim 1.5$.

Conclusions

A detailed numerical study of the two-dimensional heat-transfer problem and laminar flow around two rotating circular cylinders in side-

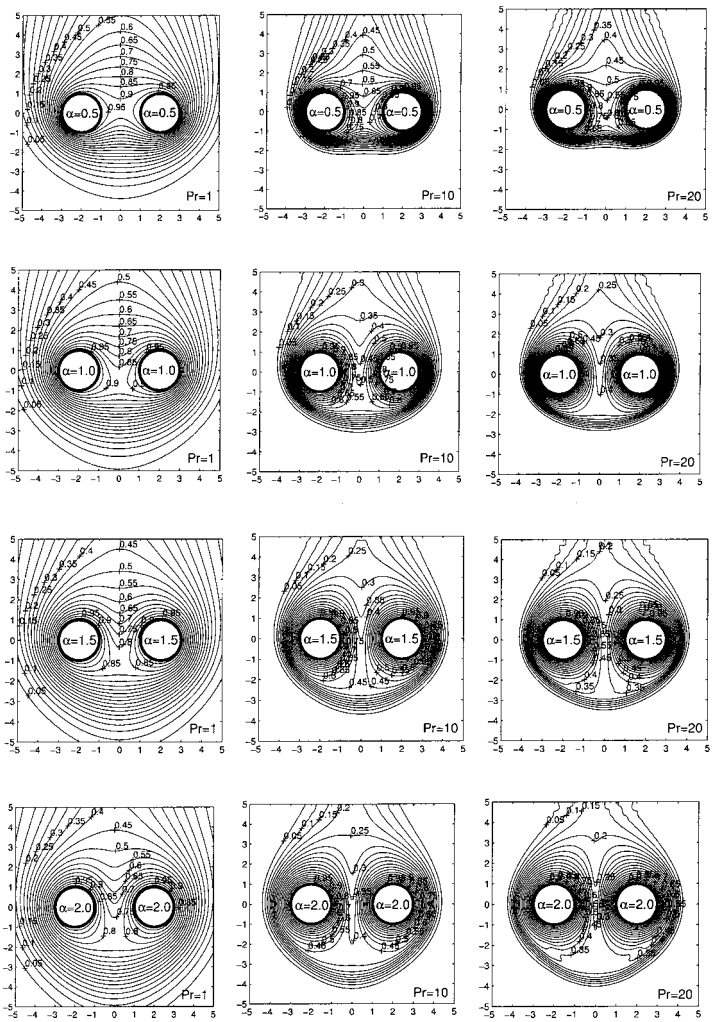

Figure 10. Temperature contours over two circular cylinders at Re = 10, g = 1, Pr = 1, 10, 20, and α = 0.5, 1.0, 1.5, and 2.0

by-side arrangement has been carried out. An efficient finite difference algorithm has been developed for the 2D Navier-Stokes equation in the cylindrical bi-polar coordinate system. Comparing the results for the case of large gap spacing with the available in the literature experimental and numerical data for the case of a single cylinder shows a good agreement,

For the problem of heat-transfer and flow around two rotating circular cylinders in side-by-side arrangement, the average Nusselt number decreases with increasing rotational speed.

For large Prandtl number (Pr = 20) and high rotational speed ($\alpha \approx 2.0$), the local Nusselt number distribution on the cylinder surfaces becomes almost uniform. This is due to the no-slip condition, the increasing rotational speed creates thick rotating layers of fluid (buffer layers) around the cylinders.

In case of small gap spacing between the cylinders, there are two flow regimes. In the first, the main stream passes through the gap between cylinders and in the second case, there is a fluid region which surrounds both cylinders and which consists of two sub-regions of closed

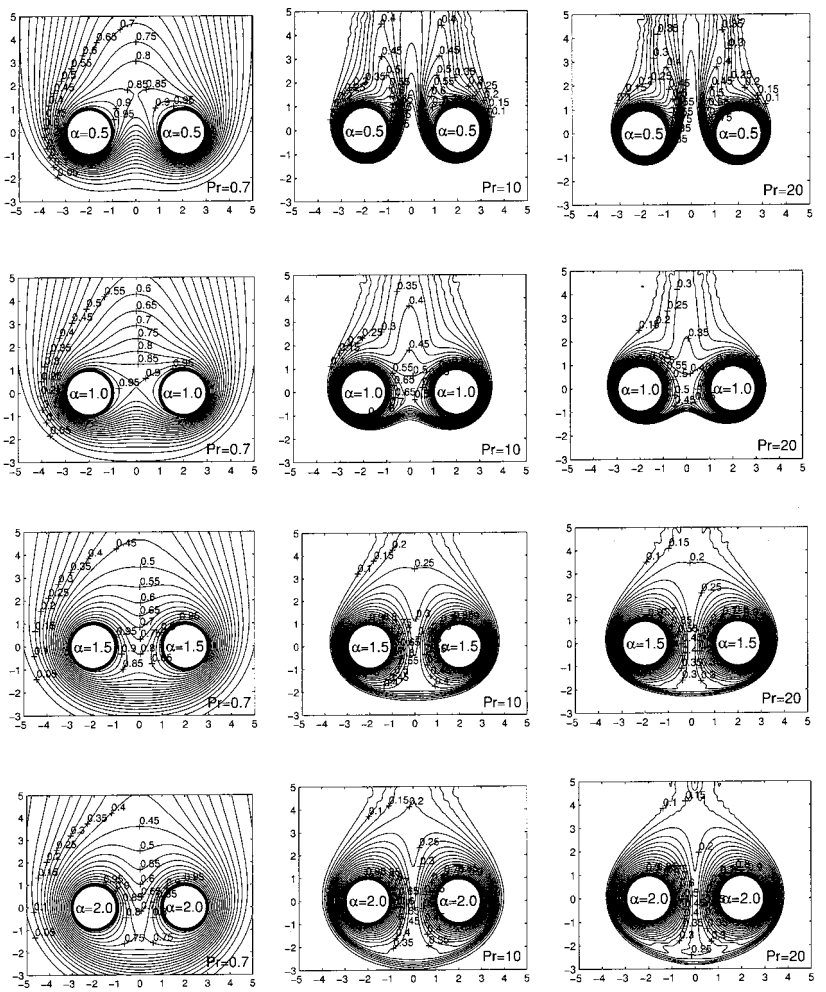

Figure 11. Temperature contours of fluid flow over two circular cylinders at *Re* = 20, *g* = 1, *Pr* = 0.7, 10, 20 and α = 0.5, 1.0, 1.5 and 2.0

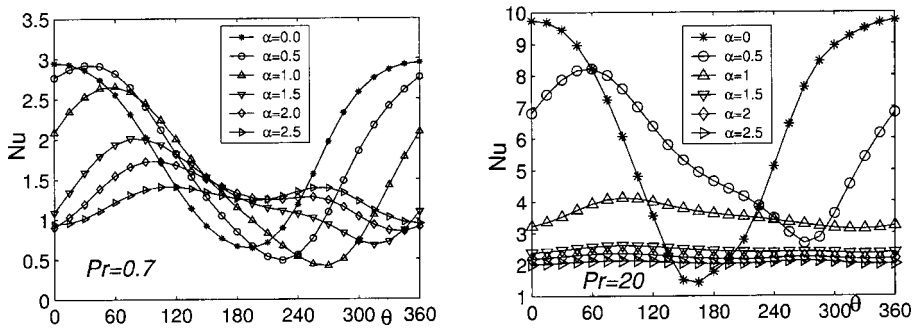

Figure 12. Local Nusselt number variation on the surface of the circular cylinders at *Re* = 20, *g* = 1 for α = 0, 0.1, 0.5, 1.0, 2.0 and 2.5; (a)- *Pr* = 0.7 and (b)-*Pr* = 20

streamlines.

It has been observed that the temperature contour pattern is similar to the streamline contour pattern. Owing to the rotation, the wake-shaped region of the isotherms is shifted in direction of the cylinder rotation. An increase in the Prandtl number increases the compactness of the isotherms toward the downstream.

References

Antontsev, S.N., Kazhikhov, A.V., and Monakhov, V.N. (1990). Boundary Value Problems in Mechanics of Nonhomogeneous Fluids. Elsevier Science Publishing Company Inc., NY.

Badr, H.M., Dennis, S.C.R., and Young, P.J.S. (1989). Steady flow past a rotating circular cylinder at low Reynolds numbers. Comput. Fluids, 17:579-609.

Batchelor, G.K., (2000). Introduction to Fluid Dynamics, Cambridge University Press.

Bharti, R.P., Chhabra, R.P., and Eswaran, V. (2007). A numerical study of the steady forced convection heat transfer from an unconfined circular cylinder. Heat Mass Transfer, 43:639-648.

Chang, K. and Song, C. (1990). Interactive vortex shedding from a pair of circular cylinders in a transverse arrangement. Int. J. Numerical Methods in Fluids, 11: 317–329.

Chung, M-H. (2006). Cartesian cut cell approach for simulating incompressible flows with rigid bodies of arbitrary shape. Computer & fluids, 35(6):607-623.

Chorin, A.J. (1968). Numerical solution of the Navier-Stokes equations. Math. Comp., 22:745-762.

Dennis, S.C.R. and Chang, G. (1970). Numerical solutions for steady flow past a Circular Cylinder at Reynolds Numbers up to 100, J. Fluid Mech., 42:47-489.

Douglas, J. and Rachford, H.H., (1956). On the numerical solution of heat conduction problems in two or three space variables. Trans. Amer. Math. Soc., 82:421–439.

Gshwendtner, M.A. (2004). Optical investigation of the heat transfer from a rotating cylinder in a cross flow. Heat and Mass Transfer, 40:561–572.

Ingham, D.B. and Tang, T. (1990). A numerical investigation into the steady flow past a rotating circular cylinder at low and intermediate Reynolds number. J. Comput. Phys., 87:91-107.

Joucaviel, M., Gosselin, L., and Bello-Ochende, T., (2008). Maximum heat transfer density with rotating cylinders aligned in cross-flow. Int. Comm. Heat Mass Transfer, 35:557-564.

Kang, S., (2003). Characteristics of flow over two circular cylinders in a side-by-side arrangement at low Reynolds numbers.

Physics of fluids, 15(9):2,486-2,498.

Kang, S., Choi, H., and Lee S. (1999). Laminar flow past a rotating circular cylinder. Physics of Fluids, 11(11):3,312-3,321.

Mahfouz, F.M. and Badr, H.M. (1999a). Heat convection from a cylinder performing steady rotation or rotary oscillation - Part I: Steady rotation. Heat and Mass Transfer, 34:365-373.

Mahfouz, F.M. and Badr, H.M. (1999b). Heat convection from a cylinder performing steady rotation or rotary oscillation - Part II: Rotary oscillation. Heat and Mass Transfer, 34:375-380.

Mittal, S. and Kumar, B. (2003). Flow past a rotating cylinder. J. Fluid Mech., 476:303–334.

Mittal, S., Kumar, V., and Raghuvanshi A. (1997). Unsteady incompressible flows past two cylinders in tandem and staggered arrangements. Int. J. Numerical Methods in Fluids, 25:1,315-1,344.

Moshkin, N. and Yambangwi, D. (2009). Steady viscous incompressible flow driven by a pressure difference in a planar T-junction channel. International Journal of Computational Fluid Dynamics, 23(3): 259-270.

Soares, A.A. and Ferreira, J.M. (2005). Flow and forced convection heat transfer in crossflow of non-newtonian fluid over a circular cylinder. Ind. Eng. Chem. Res., 44(15):5,815-5,827.

Stálberg, E., Brüger, A., Lötstedt, P., Johansson, A.V., and Henningson, D.S. (2006). High order accurate solution of flow past a circular cylinder. J. Sci. Comp., 27:431-441.

Stojkovic, D., Breuer, M., and Durst, F. (2002). Effect of high rotation rates on the laminar flow around a circular cylinder. Physics of Fluids, 14(9):3,160-3,178.

Sungnul, S. and Moshkin, N.P. (2008). Numerical simulation of flow over two rotating self-moving circular cylinders. Recent advances in computational sciences, Selected Papers from the International Workshop on Computational Sciences and Its Education Beijing; China, 29 – 31 August 2005. Palle Jorgensen, Xiaoping Shen, Chi-Wang Shu, Ningning Yan (eds). World Scientific, p. 278-296.

Sungnul, S. and Moshkin, N. P. (2006). Numerical simulation of steady viscous flow past two rotating circular cylinders. Suranaree J. Sci. Technol., 13(3):219-233.

Yanenko, N.N. (1971). The method of Fractional Steps: The Solution of Problems of Mathematical Physics in Several Variables, Translated by M. Holt., New York: Springer-Verlag.

Yoon, H.S., Kim, J.H., Chun, H.H., and Choi, H.J. (2007). Laminar flow past two rotating circular cylinders in a side-by-side arrangement. Physics of Fluids, 19(12): 128103:1-4.

Yoon, H.S., Chun, H.H., Kim, J.H., and Park, I.L.R. (2009). Flow characteristics of two rotating side-by-side circular cylinders. Computers & Fluids, 38:466-474.